Journal of Sound and Vibration (1998) **213**(1), 35–54

FILTER BANKS IMPLEMENTATION OF NUMERICAL MODELS FOR VIBROACOUSTIC ANALYSIS IN THE MEDIUM FREQUENCY RANGE

S. Gorog* and P. Micheau

G.A.U.S. Département de Génie Mécanique, Université de Sherbrooke, Sherbrooke, Québec, Canada J1K 2R1

(*Received* 12 *June* 1997, *and in final form* 12 *November* 1997)

A numerical method is proposed for predicting the vibroacoustic response of a viscoelastic structure submitted to harmonic forces in the medium frequency range. The structure is described as a finite dimension dynamical system. The frequency domain of interest is divided into several different subdomains. The method consists of solving a set of time domain equations of motion where each of them is associated with a given frequency subdomain. This time–frequency study is formulated within the framework of non-uniform modulated filter banks. Conditions are given to ensure that the analysis and the synthesis banks allow reconstruction of the complete investigated displacement field from the time solutions. A low-pass filter with a compact time support is designed to ensure an efficient computation. To illustrate the discussion, two examples using different variational approaches are proposed. First, flexural vibrations of an *in vacuo* steel plate described by a finite element method is considered. Second, a semi-analytical method is used to describe a point loaded steel plate radiating in air.

1. INTRODUCTION

In predicting the vibroacoustic response of a viscoelastic structure submitted to harmonic forces, the medium frequency domain is where the dynamical behaviour is most difficult to model. The problem lies in describing vibroacoustic phenomena for which the characteristic length is of the order of the wavelength of the excitation. Three different approaches have been proposed in the literature to describe the wave propagation properties for the medium frequency range. The first approach [1] uses complex rays to represent wave motion in the vibration structure. The second approach [2, 3] analyses the energy propagation by computing the power flow. This method results from the extension of the statistical energy analysis (S.E.A.) used to study the high frequency range [4]. The third approach [5, 6], based on a finite element model, consists of solving the dynamic equation of the structure using a time domain computation. This last method has been developed as an extension of the modal method and the direct method which are appropriate in the low frequency range [7].

The present paper deals with the third approach which is a resolution method using a matrix description of the dynamical system, for instance, resulting from a finite elements formulation or from a modal analysis. To describe the dynamic behaviour in the medium frequency range, the difficulty lies in choosing the description of the geometry of the structure as well as the model of the constitutive properties of materials. Therefore, Soize

* Corresponding author.

0022–460X/98/210035 + 20 $25.00/0/sv971425

[6] proposed to take into account structural fuzzy. Considering that such probabilistic aspects can be added, the present paper deals with a numerical tool to compute the vibroacoustic response of the studied dynamical system.

Considering the limitations of the classical modal and direct methods as the frequency increases, Soize [5] developed a computational method based on a finite element model which transforms the dynamic equation of the structure into a set of time domain equations of motion with slowly varying variables. The whole frequency range of interest is broken into several different subdomains using rectangular windows. For each given frequency subdomain, a time domain equation of motion is solved. The complete investigated response is constructed by a simple juxtaposition of the several frequency responses associated with each subdomain. However, this choice obviously implies that a cardinal sinus time window is used to analyse the excitation in each frequency subdomain. Because this function has an infinite time support, it is necessary to determine initial and final time values to integrate each time domain equation of motion numerically. Especially, the selection of a criterion to choose the initial time value is subjected to numerical difficulties [8].

An optimized solution is proposed by analysing the excitation signal with compact time suppoort windows. It is chosen to set up the method within the framework of non-uniform modulated filter banks [9–11]. This time-frequency tool is applied to construct the complete frequency displacement field of the excited structure.

Recalling the equation of motion associated with a viscoelastic structure submitted to harmonic forces, the principle of the resolution method is presented first. It is shown that the initial problem is linearized in order to work with a set of equations of motion related to the subdivision of the frequency range under interest. For each subdomain, the time domain equation of motion is solved numerically.

The analysis–synthesis banks are described in the next section. The aim is to propose the conditions which ensure perfect reconstruction. These conditions concern the set of low-pass filters used to split the frequency domain and to construct the complete response. As the vibroacoustic objective requests the computation of the frequency response, a frequency condition is given.

To simplify the computation, it is chosen to split the frequency range of interest by taking into account two consecutive subdomains only. Nevertheless, different frequency widths are considered and there must be an overlap between two successive subdomains.

The next three sections deal with the application of the method. First, the set of analysis filters is defined by using one main low-pass filter function. The condition of reconstruction allows the definition of the required synthesis filters. The choice of a causal filter function ensures that the initial conditions of the time domain intergration are verified. The second section deals with the numerical time domain integration. It is shown that two numerical parameters are required to compute the solutions. As the studied signals have bounded energy, a test on a cumulative energy quantity is proposed as a stopping criterion for the time domain integration. In the third and fourth sections, numerical results are presented to prove the accuracy and efficiency of the method. Flexural vibration of a steel plate excited by a point force is considered. Both *in vacuo* vibrations and radiation effects are studied using two different variational approaches, i.e., a finite element model and a semi-analytical model. Partial analytical results are presented in the appendices.

2. RESOLUTION METHOD

The vibroacoustic response of a linear viscoelastic structure is studied in the frequency domain assuming an exp $[j2\pi ft]$ time variation, where f and t denote respectively frequency

and time. Using a classical approach (F.E.M., B.E.M., semi-analytical methods, . . .), the structure excited by a harmonic force vector $\underline{\hat{x}}(f)$ is characterized by a mass matrix $[M(f)]$, a damping matrix $[C(f)]$ and a stiffness matrix $[K(f)]$. It is assumed that these quantities are real and frequency dependent to take into account behaviour of materials. The equation of motion associated with the displacement field $\underline{\hat{u}}(f)$ of the structure is given by

$$[\hat{Z}(f)]\,\underline{\hat{u}}(f) = \underline{\hat{x}}(f), \tag{1}$$

where $[\hat{Z}(f)] = -(2\pi f)^2[M(f)] + j2\pi f[C(f)] + [K(f)]$ is the impedance operator.

The method consists of subdividing the frequency domain into N subdomains. Each subdomain n, where $1 \leqslant n \leqslant N$, is defined in relation to a central frequency f_n and to a width Δf_n. For each frequency subdomain n, mass matrix, damping matrix and stiffness matrix are assumed to have constant values denoted by $[M_n]$, $[C_n]$ and $[K_n]$, respectively. For instance, these values can be those at the central frequency f_n. At this point, no condition has been applied on the subdividing domain.

Thus, the equation of motion (1) becomes the following system of N similar linearized equations:

$$[\hat{Z}(f, f_n)]\underline{\hat{u}}(f) = \underline{\hat{x}}(f), \qquad \forall f \in \left[f_n - \frac{\Delta f_n}{2}, f_n + \frac{\Delta f_n}{2}\right], \tag{2}$$

where the impedance operator $[\hat{Z}(f, f_n)]$ is defined by

$$[\hat{Z}(f, f_n) = -(2\pi f)^2[M_n] + j(2\pi f)\,[C_n] + [K_n]. \tag{3}$$

Each linearized frequency domain equation of motion is studied in the narrowband related to each subdomain by translating the centre of the frequency window in equation (2) from f_n to zero in the frequency domain such that

$$[\hat{Z}_n(f)]\underline{\hat{u}}_n(f) = \underline{\hat{x}}'_n(f), \qquad \forall f \in \left[-\frac{\Delta f_n}{2}, \frac{\Delta f_n}{2}\right], \tag{4}$$

with $[\hat{Z}_n(f)] = [\hat{Z}(f + f_n, f_n)]$, $\underline{\hat{u}}_n(f) = \underline{\hat{u}}(f + f_n)$ and $\underline{\hat{x}}'_n(f) = \underline{\hat{x}}(f + f_n)$.

By applying the inverse Fourier transform over the whole frequency domain but where the only non-zero values are located in the interval $[-\Delta f_n/2, \Delta f_n/2]$, each equation of motion given by equations (4) is equivalent to a time domain equation as follows:

$$[M_n]\frac{\mathrm{d}^2\underline{u}_n(t)}{\mathrm{d}t^2} + [\tilde{C}_n]\frac{\mathrm{d}\underline{u}_n(t)}{\mathrm{d}t} + [\tilde{K}_n]\underline{u}_n(t) = \underline{x}'_n(t). \tag{5}$$

with $[\tilde{C}_n] = [C_n] + 4j\pi f_n\,[M_n]$ and $[\tilde{K}_n] = [K_n] - (2\pi f_n)^2[M_n] + j2\pi f_n\,[C_n]$.

The time excitation signal denoted by $\underline{x}'_n(t)$ is the frequency translated excitation and the time signal $\underline{u}_n(t)$ is the frequency translated displacement field.

The proposed method consists of solving the ordinary differential time domain equation of motion (5) numerically. For this purpose, any direct unconditionally stable step by step time integration algorithm can be used. It is chosen to apply a Newmark scheme. According to the sampling theorem, the response $\underline{u}_n(t)$ can be described without loss of information from its numerical values at times $t = kT_n$ with $T_n = 1/\Delta f_n$ and $k \in \mathbb{Z}$ if $|\underline{\hat{u}}_n(f)| = 0$ for $|f| > \Delta f_n$. The main interest of the method is to work with low-frequency excitation signals. Since a frequency linearization is used, the investigated displacement field is found by computing low frequency signals. Consequently, the narrow subdomain $[-\Delta f_n/2, \Delta f_n/2]$ is a low-pass frequency range. The problem is then to reconstruct the

complete response $\underline{\hat{u}}(f)$, solution of equation (1), from the N time domain solutions $\underline{u}_n(kT_n)$.

3. ANALYSIS AND SYNTHESIS BANKS

The excitation signal $\underline{x}(t)$ related to $\underline{\hat{x}}(f)$ (equation (1)) must be broken into N different signals $\underline{\hat{x}}'_n(t)$. This process has to be reversible in order to reconstruct the complete displacement field of the structure from the N time solutions of equation (5). For this purpose, it is chosen to use non-uniform filter banks to divide the excitation into subdomains and then to recover the complete solution. Figure 1 illustrates the proposed approach.

To apply the analysis bank, the frequency spectrum of the time domain excitation $\underline{x}(t)$ is shifted towards the origin by f_n which is known to be the demodulation frequency. The resulting shifted complex signal is passed through a low-pass filter g_n having a cutoff frequency of Δf_n. This low-pass complex signal, denoted by $\underline{x}_n(t)$, is used instead of $\underline{x}'_n(t)$ as the excitation in the linearized model described by equation (5). Therefore, the applied filtered excitation signal resulting from the analysis bank is defined as

$$\underline{x}_n(t) = \underline{x}(t) \exp[-j2\pi f_n t] \otimes g_n(t), \tag{6}$$

where $\otimes$ denotes the convolution operator. The frequency spectrum of signal $\underline{x}_n(t)$ has the approximated compact support $[-\Delta f_n/2, \Delta f_n/2]$.

The synthesis bank allows reconstruction of the complete displacement field $\underline{u}^r(t)$ from the time domain solutions $\underline{u}_n(t)$ (equation (5)). By applying the sampling theorem, the calculated response $\underline{u}_n(t)$ is sampled at the rate $T_n = 1/\Delta f_n$ to reduce aliasing. Therefore, the numerical values of the solution of equation (5) provide a sampled complex signal $\underline{u}^e_n(t)$. The synthesis bank is applied using a set of low-pass filters h_n. Each sampled complex signal is filtered and then shifted back into the frequency domain from the origin to f_n. The operation involved in this reconstruction is complementary to the one used in the

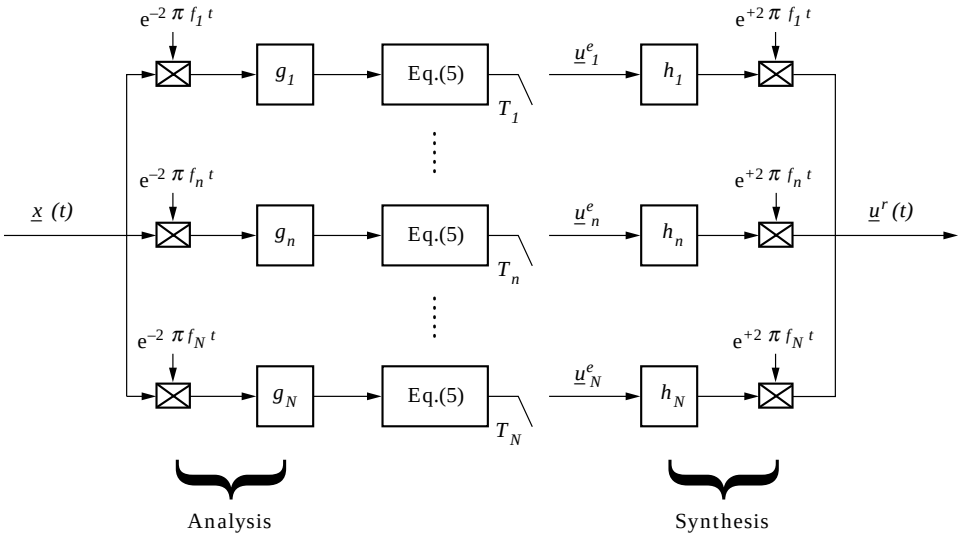

Figure 1. Algorithm proposed using analysis filter bank (g), time domain equation of motion (5) and synthesis filter bank (h).

analysis bank. The resulting reconstructed displacement field $\underline{u}^r(t)$ is obtained from a summation on the number of subdomains as follows:

$$\underline{u}^r(t) = \sum_n T_n \left[\underline{u}_n^e(t) \otimes h_n(t)\right] \exp\left[j2\pi f_n t\right]. \tag{7}$$

Equation (7) gives the classical time domain construction of modulated filter banks. The chosen set of filters g_n and h_n is known as a complementary Euclidian set [9].

Keeping in mind the vibroacoustic objective, the frequency response $\hat{\underline{u}}^r(f)$ must be calculated. Thus, the Fourier transform of equation (7) leads to

$$\hat{\underline{u}}^r(f) = \sum_n T_n \hat{\underline{u}}_n^e(f - f_n)\hat{h}_n(f - f_n). \tag{8}$$

The presented analysis–synthesis method allows it to be ensured that the solution $\hat{\underline{u}}^r(f)$ is the frequency response to a reconstructed excitation $\hat{\underline{x}}^r(f)$ such that

$$\hat{\underline{u}}^r(f) = [\hat{Z}(f)]^{-1}\hat{\underline{x}}^r(f). \tag{9}$$

The excitation force $\hat{\underline{x}}^r(f)$ results from the application of both analysis and synthesis filters. It is now important to ensure that equation (9) is equivalent to the studied equation of motion (1). As shown in Appendix A, this requires that the set of filters g_n and h_n verify the following perfect reconstruction condition:

$$\sum_{n=1}^{N} \hat{g}_n(f - f_n)\hat{h}_n(f - f_n) = 1. \tag{10}$$

Consequently, the reconstructed excitation force is the applied force such as $\hat{\underline{x}}^r(f) = \hat{\underline{x}}(f)$. Then, the solution $\hat{\underline{u}}^r(f)$ is the investigated solution $\hat{\underline{u}}(f)$ of equation (1). The application of equation (10) obviously depends on the way used to break the frequency range into N subdomains.

4. DIVISION OF THE FREQUENCY DOMAIN

The displacement field solution is computed in the frequency domain in order to evaluate the vibroacoustic indicators. By solving the N frequency shifted systems (equation (4)), the aim of the computation is to obtain the complete response of the structure for a given frequency range extending from a minimum frequency f_{min} to a maximum frequency f_{max}. This response is reconstructed if the following condition is verified:

$$[f_{min}, f_{max}] \subset \left(\bigcup_{n=1}^{N} \left[f_n - \frac{\Delta f_n}{2}, f_n + \frac{\Delta f_n}{2} \right] \right). \tag{11}$$

In the following, the frequency f is therefore always included in the studied domain $[f_{min}, f_{max}]$. From a theoretical point of view, any frequency discretization can be used to decompose the frequency domain. Nevertheless, to ensure simple and convenient computation, it is chosen to limit the overlap between the different subdomains as follows:

$$\forall n, \qquad f_{n+1} - f_n \geqslant \frac{\Delta f_{n+1}}{2}, \tag{12}$$

$$f_{n+1} - f_n \geqslant \frac{\Delta f_n}{2}, \tag{13}$$

$$f_{n+1} - f_n < \frac{\Delta f_n}{2} + \frac{\Delta f_{n+1}}{2}. \tag{14}$$

Equations (12) and (13) impose that there should never be an overlap of more than two subdomains. When the equalities are verified, both subdomains have identical width. The third condition (14) imposes that there should always be a non-zero overlap between two consecutive subdomains. For identical width, this overlap occurs completely between the two central frequencies, i.e., on each half width.

Assuming that equations (12)–(14) are verified, the condition given by equation (10) reduces to

$$\hat{g}_n(f - f_n)\hat{h}_n(f - f_n) + \hat{g}_{n+1}(f - f_{n+1})\hat{h}_{n+1}(f - f_{n+1}) = 1, \qquad \forall f \in [f_n, f_{n+1}]. \tag{15}$$

Since an overlap must occur, three frequency ranges have to be separated between the two successive central frequencies f_n and f_{n+1} to apply equation (15).

According to equations (12) and (13), for the first $[f_n, f_{n+1} - \frac{1}{2}\Delta f_{n+1}]$ and the third $[f_n + \frac{1}{2}\Delta f_n, f_{n+1}]$ range, the calculated response is the solution computed for the two subdomains n and $n+1$, respectively. Consequently, condition (15) gives

$$\hat{h}_n(f - f_n) = \frac{1}{\hat{g}_n(f - f_n)}, \qquad \forall f \in [f_n, f_{n+1} - \tfrac{1}{2}\Delta f_{n+1}]; \tag{16}$$

$$\hat{h}_{n+1}(f - f_{n+1}) = \frac{1}{\hat{g}_{n+1}(f - f_{n+1})}, \qquad \forall f \in [f_n + \tfrac{1}{2}\Delta f_n, f_{n+1}]. \tag{17}$$

According to equation (14), for the second range $[f_{n+1} - \frac{1}{2}\Delta f_{n+1}, f_n + \frac{1}{2}\Delta f_n]$, the solution depends on the two calculated solutions for the subdomains n and $n+1$. The influence of each subdomain on the overlapping band is described using the maximum likelihood principle which ensures a smooth transition. In that case, equation (15) gives

$$\left.\begin{aligned} \hat{h}_n(f - f_n) &= \frac{\hat{g}_n^*(f - f_n)}{|\hat{g}_n(f - f_n)|^2 + |\hat{g}_{n+1}(f - f_{n+1})|^2} \\ &\text{and} \\ \hat{h}_{n+1}(f - f_{n+1}) &= \frac{\hat{g}_{n+1}^*(f - f_{n+1})}{|\hat{g}_n(f - f_n)|^2 + |\hat{g}_{n+1}(f - f_{n+1})|^2} \end{aligned}\right\} \forall f \in [f_{n+1} - \tfrac{1}{2}\Delta f_{n+1}, f_n + \tfrac{1}{2}\Delta f_n], \tag{18}$$

where * designates the complex conjugate and $\|$ the magnitude.

By applying the three conditions given by equations (16)–(18), the complete displacement field solution defined by equation (8) is easily computed as presented in Appendix B.

For the case where the frequency width is the same for all subdomains, such that $\Delta f_n = \Delta f$, only one filter g and one filter h are needed. In that case, according to the conditions given by equations (12)–(14), no weight function is used because the overlap concerns the overall subdomain from f_n to f_{n+1}. Nevertheless, it can be noted that, if necessary, the present method can be applied to study a partial overlap for identical width.

5. PROTOTYPE FILTER

The algorithm of the method has been presented from a signal processing point of view. The last point concerns the choice of the low-pass filters g_n or h_n. According to equations (16)–(18), it is sufficient to choose one set of filters only, for instance,

$\{g_n(t), n = 1, \ldots, N\}$. As a Newmark scheme is applied to solve equation (5), it is ensured that all low-pass filter functions $g_n(t)$ will obey the zero intital conditions of time domain integration.

To simplify the numerical implementation, a mother causal filter g_0 of compact time support has been chosen to define the low-pass filters g_n by use of a dilation coefficient α_n such that

$$g_n(t) = g_0\left(\frac{t}{\alpha_n}\right) \quad \text{and} \quad \hat{g}_n(f) = \alpha_n \hat{g}_0(\alpha_n f).$$

Thus, the frequency width Δf_n of each subdomain n is given in terms of the frequency support $\Delta f_0 = 1/T_0$ of the Fourier transform $\hat{g}_0(f)$ as follows:

$$\Delta f_n = \frac{\Delta f_0}{a_n} \quad \text{and therefore} \quad T_n = \alpha_n T_0.$$

The Fourier transform $\hat{g}_n(f)$ is low-pass over the range $[-\frac{1}{2}(\Delta f_o/\alpha_n), \frac{1}{2}(\Delta f_0/\alpha_n)]$.

It is worth pointing out that the choice of a causal filter with a time compact support eliminates the problem of defining a beginning criterion for the time domain integration. Therefore, this choice always verifies the initial conditions of the numerical scheme. Moreover, the choice of a causal excitation allows the sampling values to be computed at positive times only.

According to the previous analysis, the proposed filter function $g_0(t)$ is defined by

$$g_0(t) = a_0 + a_1 \cos\left[\frac{2\pi t}{6T_0}\right] + a_2 \cos\left[\frac{4\pi t}{6T_0}\right], \quad \forall t \in [0; 6T_0],$$

$$g_0(t) = 0, \quad \text{elsewhere}, \tag{19}$$

with the following optimized coefficients: $a_0 = 0{\cdot}5786$, $a_1 = -1{\cdot}052$ and $a_2 = 0{\cdot}4734$. Figure 2 shows the impulse response of the filter $g_0(t)$ versus a time normalized with respect to T_0.

Coefficients a_0, a_1 and a_2 must verify

$$a_0 + a_1 + a_2 = 0, \tag{20}$$

in order to ensure that the initial conditions of zero value and zero first derivative needed by the Newmark scheme are verified.

According to the frequency analysis, the Fourier transform $\hat{g}_0(f)$ of $g_0(t)$ (equation (19)) is used as given by

$$\begin{aligned}\hat{g}_0(f) = \{&a_0 \operatorname{sinc}[f6T_0] \exp[-j\pi f6T_0] \\ &- \frac{a_1}{2} \operatorname{sinc}[f6T_0 - 1] \exp[-j\pi(f6T_0 - 1)] \\ &- \frac{a_1}{2} \operatorname{sinc}[f6T_0 + 1] \exp[-j\pi(f6T_0 + 1)] \\ &+ \frac{a_2}{2} \operatorname{sinc}[f6T_0 - 2] \exp[-j\pi(f6T_0 - 2)] \\ &+ \frac{a_2}{2} \operatorname{sinc}[f6T_0 + 2] \exp[-j\pi(f6T_0 + 2)]\} 6T_0,\end{aligned} \tag{21}$$

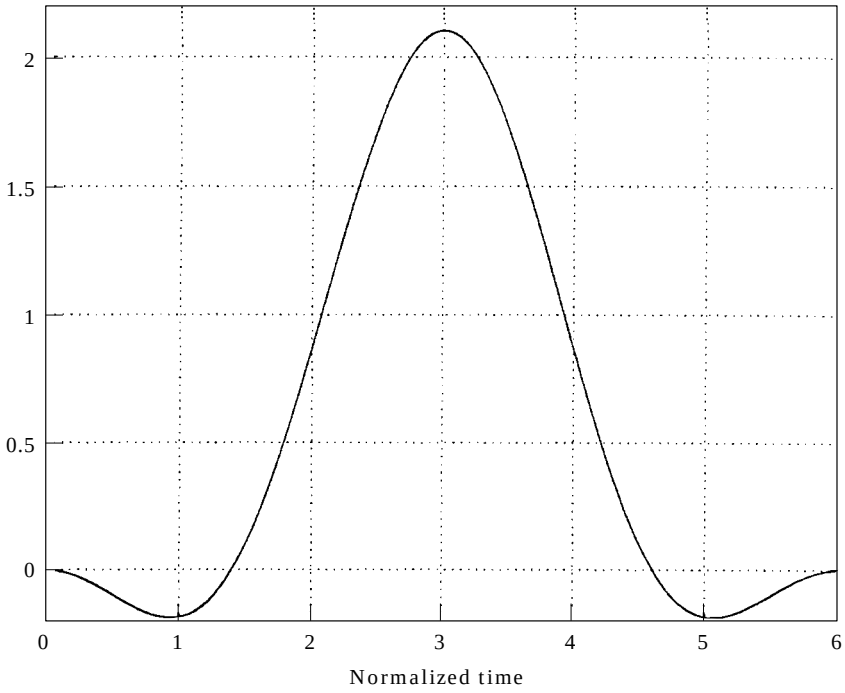

Figure 2. Prototype low-pass analysis filter $g_0(t/T_0)$.

where the cardinal sine function is defined by: $\forall y$ real, $\text{sinc}[y] = \sin[\pi y]/(\pi y)$.

Figure 3 shows the magnitude of the function $\hat{g}_0(f)$ versus a normalized frequency with respect to Δf_0. According to the frequency range of each shifted subdomain, the useful part of the magnitude lies between $-1/2$ and $1/2$. Outside this region, the attenuation is greater than 30 dB and this is considered sufficient to apply the sampling theorem.

6. NUMERICAL TIME DOMAIN INTEGRATION

For each subdomain, the differential equation given by equation (5) is solved numerically using a Newmark scheme. This time domain integration has to be computed for every positive and negative times. However, according to the causal property of the presented analysis–Newmark–synthesis process, the investigated response is zero for the negative times, i.e., the excitation occurs for positive times only. Thus, the numerical integration requires determination of two time parameters.

First, a time increment δt has to be specified to compute the time solution step by step. To simplify the numerical implementation, this time increment is defined by dividing the sampling time T_n by a non-zero integer m_T as follows:

$$\delta t = \frac{T_n}{m_T} \quad \text{with} \quad m_T > 0. \tag{22}$$

This is equivalent to dividing T_n into δt regular steps. Hence, the positive non-zero integer m_T constitutes a given numerical parameter of the method. For the unit value, the solution is computed at sampling time only.

Second, a final time t_F has to be found for stopping the numerical integration. It is chosen to obtain the final time by applying a numerical test on an energetic quantity associated

with the signals $\underline{u}_n(t)$. Recall that the global energy balance applied to the structure indicates that the viscous dissipated energy over the whole frequency range has a finite value. In the present numerical approach, this global energy is related to the reconstructed displacement field taking into account the overlap between the different subdomains. To stop the time domain integration, the difficulty lies in defining an energy quantity related to the particular response of the structure for the nth subdomain which does not represent the complete response. It is proposed to use an equivalent dissipated energy E_n^d related to the displacement field solution of each subdomain n such that

$$E_n^d = \int_{-\infty}^{\infty} D_n(t)\,\mathrm{d}t < \infty, \tag{23}$$

where $D_n(t)$ is a time domain dissipated power defined in relation to the viscous damping matrix $[C_n]$ as follows:

$$D_n(t) = \tfrac{1}{2}\,\underline{r}_n(t)^T \cdot [C_n] \cdot \underline{r}_n^*(t). \tag{24}$$

The signal $\underline{r}_n(t)$ represents the velocity field for the narrow low-frequency range: $\underline{r}_n(t) = \underline{v}_n(t) + j2\pi f_n\,\underline{u}_n(t)$. The velocity $\underline{v}_n(t)$ is directly computed by applying the Newmark scheme to equation (5).

It follows that the total dissipated energy related to the structure is an unknown function of the different energy quantities E_n^d defined for each frequency subdomain n. However, by reducing the overlap to a null frequency range and by choosing an ideal low-pass filter, the calculated dissipation E_n^d tends to the physical value of the dissipation energy in the given frequency subdomain n.

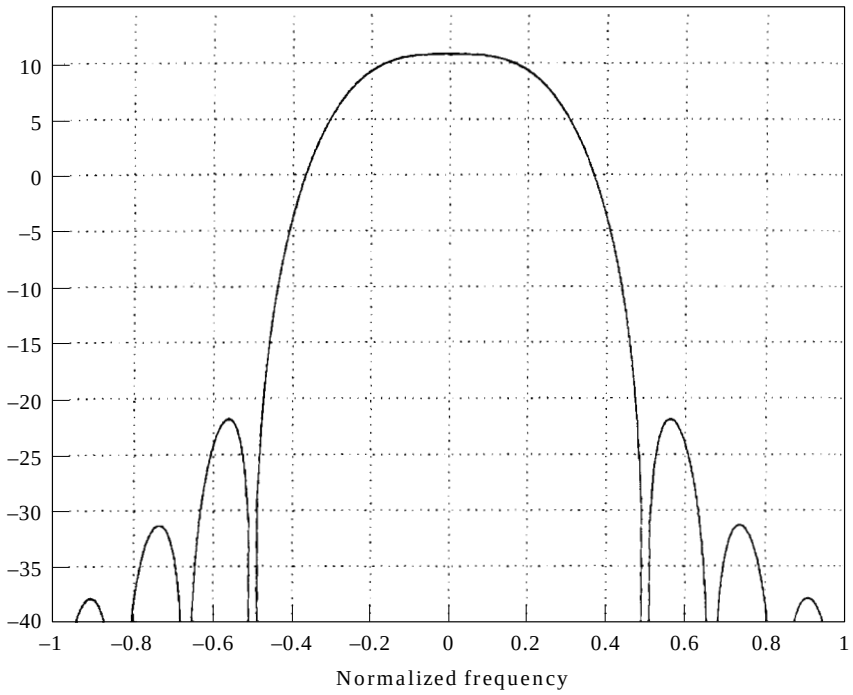

Figure 3. Magnitude of the Fourier transform $\hat{g}_0(f/\Delta f_0)$ of the prototype low-pass analysis filter.

The numerical test chosen to stop the time integration is applied on the bounded energy E_n^d. The integral of equation (23) is evaluated by computing a cumulated dissipation power in the time domain. The test is used to verify that this sum tends to a limit value. Hence, the power quantity D_n defined by equation (24) is computed for each time step to obtain the cumulated power P_c as follows:

$$P_c(k) = \sum_{i=0}^{k} D_n\left(\frac{iT_n}{m_T}\right). \tag{25}$$

The zero value of the integer step i designates the initial time of the integration. The test criterion is on the magnitude of the first variation of P_c (equation (25)) to find the limit value which indicates that the end of the time integration is reached. The numerical requirement leads to compare this variation to an error value Υ for each time step, such that

$$\frac{P_c(k+1) - P_c(k)}{P_c(k+1)} \leqslant \Upsilon. \tag{26}$$

When equation (26) is verified for a given error value Υ, the last value of k characterizes the end of the time integration. This value allows the number m_F of time samples required to compute the solution to be known. The final time t_F of the integration is given by $t_F = m_F T_n$. The smaller is the error value Υ, the larger is the value of m_F and hence the larger is the duration of the time domain integration.

The choice of the criterion can now be discussed. For instance, as the filter has a compact time support, energy of the excitation related to each subdomain can easily be calculated if the impulse response is studied. Therefore, a criterion would be defined by comparing the time dissipated energy value to the time excitation energy value. However, the chosen criterion seems to be convenient for any realistic bounded energy excitation.

The presented numerical time integration needs $(m_F m_T + 1)$ time increments δt (equation (22)). This number has to be kept in mind because a trade off exists between the quality of the response signal and the computing requirement in terms of CPU time and memory resources. It follows that the values of parameters m_T and Υ have to be sufficient to ensure that an accurate computation of equation (5) is obtained. Especially, a low value of Υ is needed to take into account the major part of the response. It is clear that a large value of Υ cuts out the time integration too early and hence, leads to a loss of informations on of the response. The influence of the time step m_T is less important but also exists. For low values of m_T, the computation gives a weak approximation of the solution of the differential equation (5). Consequently, the precision of the numerical results depends on the two parameters m_T and Υ.

7. VALIDATION USING A FINITE ELEMENT METHOD

In this first example, matrices describing the structure are obtained by a classical finite element method. The damping matrix $[C(f)]$ is replaced by the stiffness matrix $[K(f)]$ using a loss factor η. Accordingly, for each subdomain n, the impedance operator of equation (3) becomes

$$[\hat{Z}(f, f_n)] = -(2\pi f)^2[M_n] + [K_n](1 + j\eta).$$

The present case deals with the flexural vibrations of a point loaded steel plate. Geometry and boundary conditions are given in Figure 4. The thickness of the plate is $h = 0{\cdot}01$ m. Steel is characterized by a Young's modulus $E = 2 \times 10^{11}$ Pa, a Poisson ratio

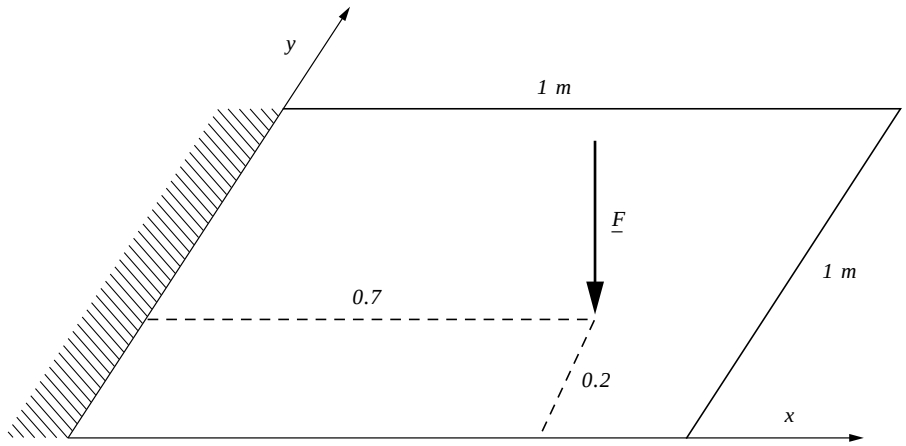

Figure 4. *In vacuo* steel plate clamped on one side, excited to harmonic flexure force F.

$v = 0{\cdot}3$ and a density $\rho = 7800\ \text{kg/m}^3$. The loss factor is $\eta = 0{\cdot}01$. The finite element mesh contains 40×40 elements. Using the classical finite element method criterion of six elements per wavelength, such a mesh is valid for a frequency domain of 800–4000 Hz.

The response of the plate is evaluated by computing the mean square velocity which refers to a spatial average over the plate surface. It is chosen to compare the numerical results with the solution given by a direct computation of equation (1). Results could also be compared with a modal method because matrices do not depend on frequency. However, modal methods are not appropriate in the medium frequency range, while direct

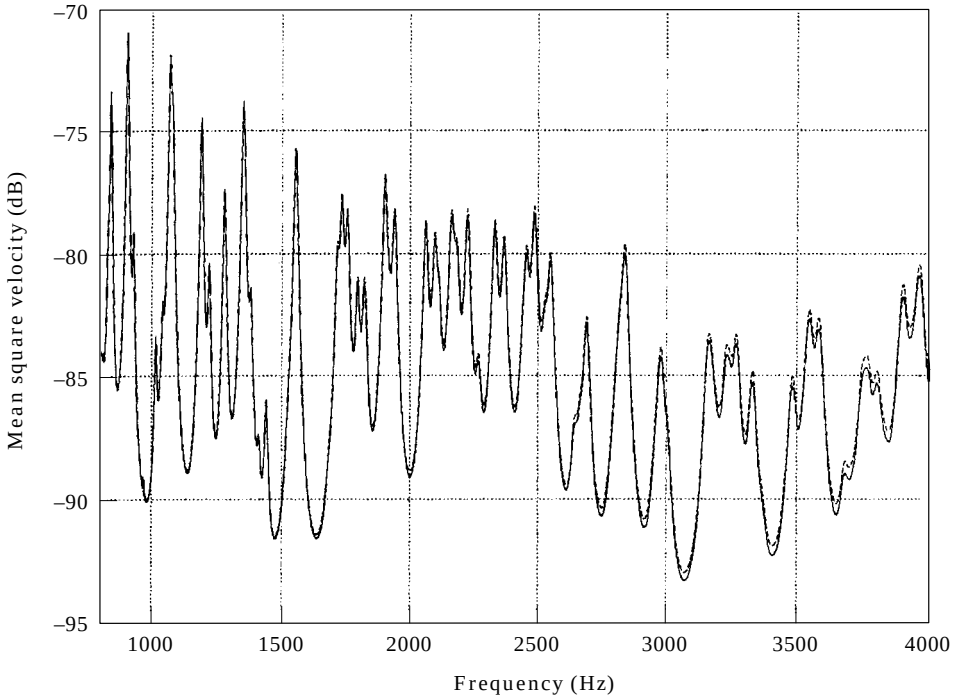

Figure 5. Comparisons of the mean square velocity of the *in vacuo* steel plate obtained by the proposed filter bank method (——) and by a direct method (- - - -).

TABLE 1

Comparative values for different number N of frequency subdomains with $m_T = 10$ *and* $\Upsilon = 10^{-6}$ *for the in vacuo plate*

N	12	17	33	81	120	321	640
Δf (Hz)	581·82	400	200	80	53·78	20	10
Relative CPU time (%)	6	6	7	10	12	17	50
m_F max	117	82	44	22	16	9	7

computation is classically used in this range. The results are presented in Figure 5. A perfect agreement between the two solutions is obtained.

The proposed analysis–synthesis method needs to break the whole frequency domain into several subdomains. Using assigned values for both numerical parameters m_T and Υ, i.e., $m_T = 10$ and $\Upsilon = 10^{-6}$, the following discussion deals with the choice of the subdivision scheme and of the overlapping of the frequency subdomains. The main objective is to show the influence of this choice on the performance of the method in terms of CPU time and memory resources.

Using identical widths for each frequency range such that $\Delta f_n = \Delta f, \forall n$, the effect of the number N of subdomains has been studied as indicated in Table 1. Resulting CPU times are given as a percentage relative to the CPU time given by the direct computation of equation (1). The main result is that the presented method is faster than the direct computation. Table 1 shows that as the number of subdomains increases, CPU time also increases. Consequently, by computing more and more subdomains, the limiting CPU time would tend to that of the direct method giving the displacement field for each frequency. The main reason to explain why the presented method can be faster is that the impedance operator of equation (1) has to be calculated for every frequency in a direct approach while matrices of equation (5) have to be evaluated only once for each subdomain.

However, the presented values indicate that a lower limit exists on the rapidity of the computation. Below a given number of subdomains, for instance 33, no more CPU time can be gained. Memory requirements can be evaluated from the number m_F of samples computed for each subdomain. It is related to the final time value such that $t_F = m_F / \Delta f$. Moreover, by reducing the number of subdomains, the width Δf increases. For instance, it can be doubled as demonstrated by the two cases $N = 17$ and $N = 33$ (Table 1). Nevertheless, for these two cases, the time domain computation for the first two subdomains takes a similar duration of integration. According to the different time sampling rates, it follows that the number m_F is greater for $N = 17$ than for $N = 33$. This number has a great importance for optimizing the memory resources taken by the Newmark scheme. To construct the global solution, both displacement field values and velocity field values are required at each time sample. Hence, the dimension of resulting complex vectors is the product of the number of finite element nodes by the number m_F of time samples. Therefore, to limit the memory requirement, it appears more interesting to choose more subdomains for a comparable CPU time. Nevertheless, the present computation method can require almost twice the memory resources of the direct computation.

To illustrate the time domain integration, Figure 6 shows the time domain power defined by equation (24) and the cumulated dissipation power of equation (25) as a function of time for $N = 33$ frequency subdomains of identical width. The plotted curves are limited to five subdomains only for clarity but all curves are similar. It is shown that for lower frequency ranges where resonance peaks have great amplitudes (Figure 5), a long

duration of time domain integration is needed while for higher frequency ranges, the time domain duration is shorter. it is worth pointing out that the different values of time domain powers indicate the frequency range where the structure would be more likely to vibrate.

Because the problem lies in the computation in low frequency ranges, previous results point out that a non-uniform filter bank is more appropriate to optimize the numerical requirements. For instance, it is chosen to break the frequency domain into $N = 18$

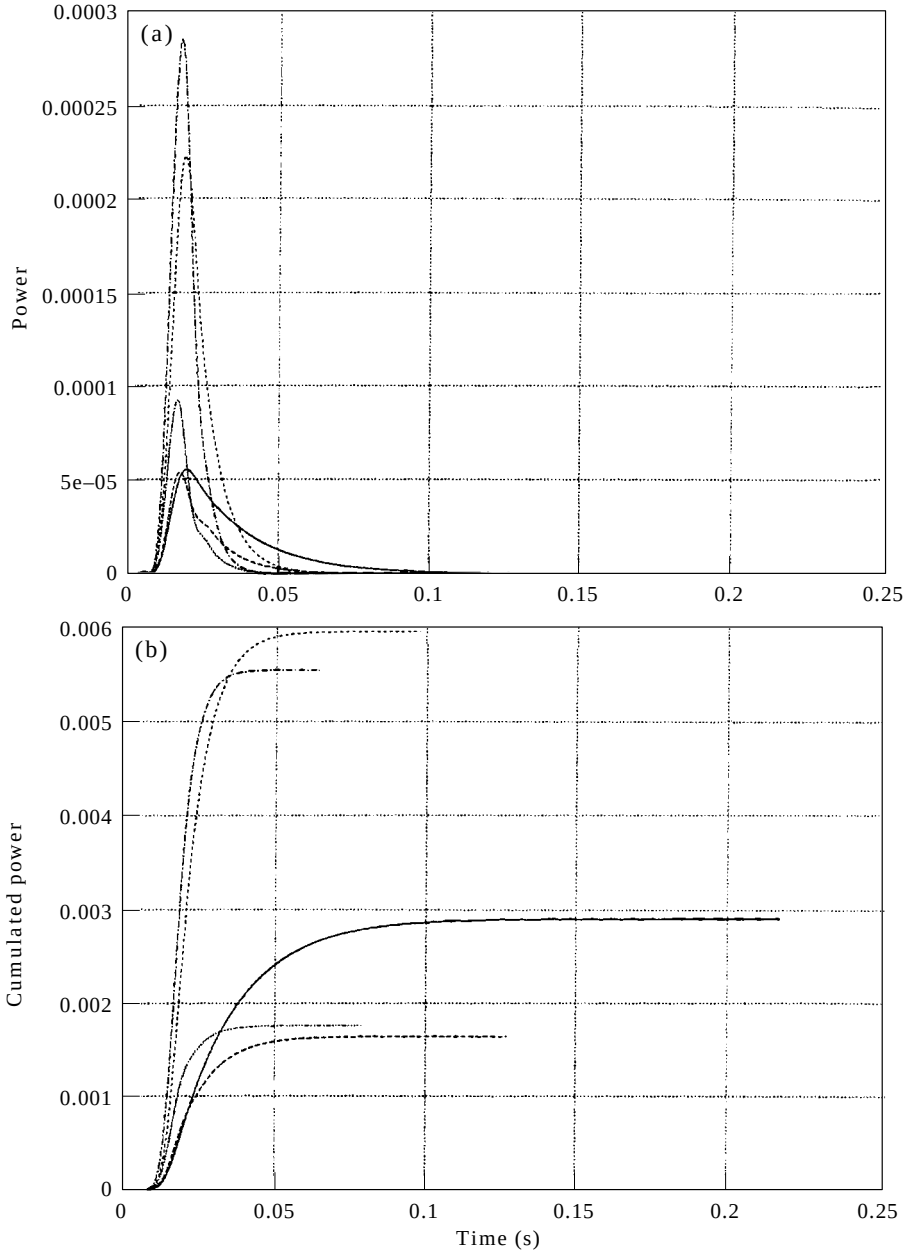

Figure 6. (a) Five time domain powers and (b) cumulated powers for the frequency division into $N = 33$ frequency subdomains of identical width for the case of the *in vacuo* plate referring to subdomains 1 (——), 8 (— — —), 15 (——), 22 (. . .) and 33 (–·–).

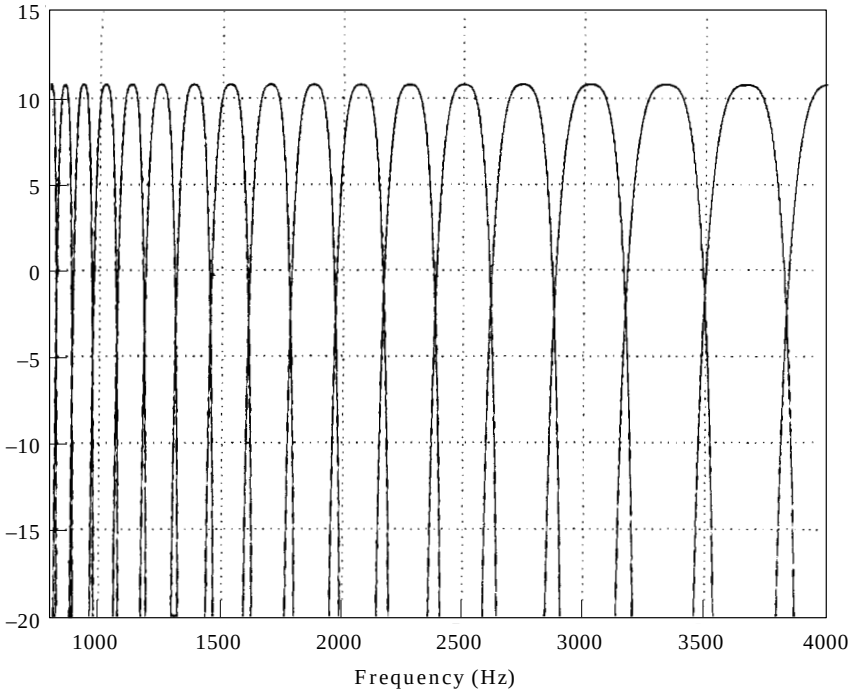

Figure 7. Non-uniform analysis filter bank.

frequency subdomains having different widths Δf_n as indicated in Table 2. Using this frequency division, relative CPU time reaches 4% and the number m_F stays in a small range of values over the complete frequency domain. Hence, numerical requirements have been improved. Time domain cumulated powers depend on the different time sampling rates as shown in Figure 8. Curves are shifted to the right when compared to Figure 6 as the frequency width Δf_n decreases.

8. VALIDATION USING A SEMI-ANALYTICAL METHOD

This second example deals with the flexural vibration of a point loaded steel plate radiating in air. The radiation effect is modelled as a frequency-dependent added mass and added damping on the structure. A semi-analytical approach computing Rayleigh integrals

TABLE 2

Non-uniform division into $N = 18$ *frequency subdomains with* $m_T = 10$, $\Upsilon = 10^{-6}$ *for the in vacuo plate. Relative CPU time becomes* 4%

n	1	2	3	4	5	6	7	8	9
Δf_n(Hz)	60	80	100	120	140	160	180	200	220
f_n(Hz)	800	855	930	1020	1125	1245	1380	1530	1695
m_F	18	21	23	23	25	26	27	26	26
n	10	11	12	13	14	15	16	17	18
Δf_n(Hz)	240	260	280	300	340	380	420	430	440
f_n(Hz)	1875	2070	2275	2500	2745	3025	3335	3660	4000
m_F	26	25	25	25	25	25	26	24	23

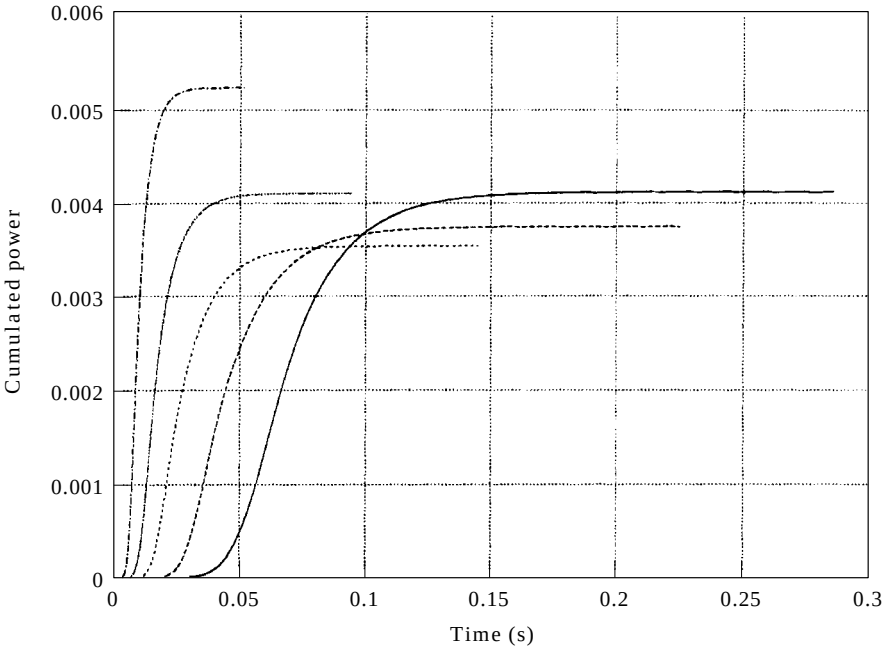

Figure 8. Five time domain cumulated powers for the non-uniform division into $N = 18$ frequency subdomains for the case of the *in vacuo* plate referring to subdomains 1 (——), 3 (— — —), 7 (– – –), 11 (. . . .) and 18 (–·–).

[12] is used to define the frequency dependent matrices of the vibroacoustic system (equation (1)).

Boundary conditions are given on Figure 9. Dimensions of the rectangular plate are $L_x = 1{\cdot}4$ m, $L_y = 1$ m and $L_z = 0{\cdot}01$ m. The point force is located at $x = 0{\cdot}1$ m, $y = 0{\cdot}1$ m. Steel properties were given in the previous section. The loss factor of the plate is $\eta = 0{\cdot}01$. The air is characterized by density $\rho_{air} = 1{\cdot}2$ kg/m^3 and sound velocity $c_{air} = 344{\cdot}8$ m/s.

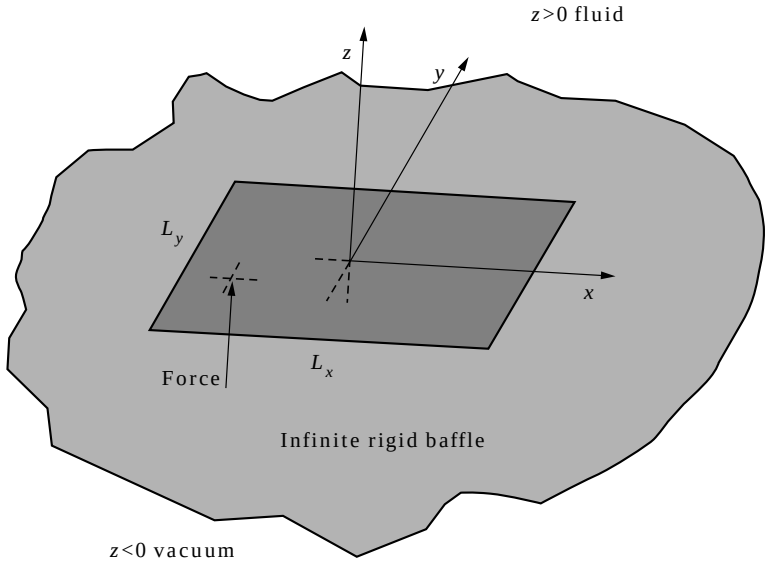

Figure 9. Simply supported baffled steel plate submitted to harmonic point force.

TABLE 3

Non-uniform division into $N = 21$ frequency subdomains with $m_T = 10$, $\Upsilon = 10^{-6}$ for the radiating plate

n	1	2	3	4	5	6	7	8	9	10	
Δf_n(Hz)	60	65	70	75	80	85	90	95	100	110	
f_n(Hz)	500	553	605	663	725	795	870	945	1025	1115	
m_F	52	52	52	44	37	40	36	23	19	14	
n	11	12	13	14	15	16	17	18	19	20	21
Δf_n(Hz)	120	140	160	180	200	220	240	260	280	300	300
f_n(Hz)	1210	1320	1450	1590	1750	1920	2110	2310	2530	2770	3000
m_F	14	14	14	17	20	22	25	27	29	31	31

The critical frequency is used to separate the weak radiation effect from the strong radiation effect [12]. For the case presented, this critical frequency is around 1300 Hz. The method presented has been applied in a frequency range of 500–3000 Hz to study both effects. The mean square velocity referring to a spatial average over the radiating plate surface is computed as the vibroacoustic indicator.

According to previous results, solutions in low frequency subdomains are computed with narrow bandwidths and solutions in high frequency subdomains are computed with large ones. This progressive frequency subdivision is given in Table 3.

Results given in Figure 10 are compared to a step by step frequency computation of equation (1). An excellent agreement is obtained below as well as above the critical frequency. It is worth recalling that the solution obtained is equal to the solution of the direct method at central frequencies only. Between two central frequencies, solutions are

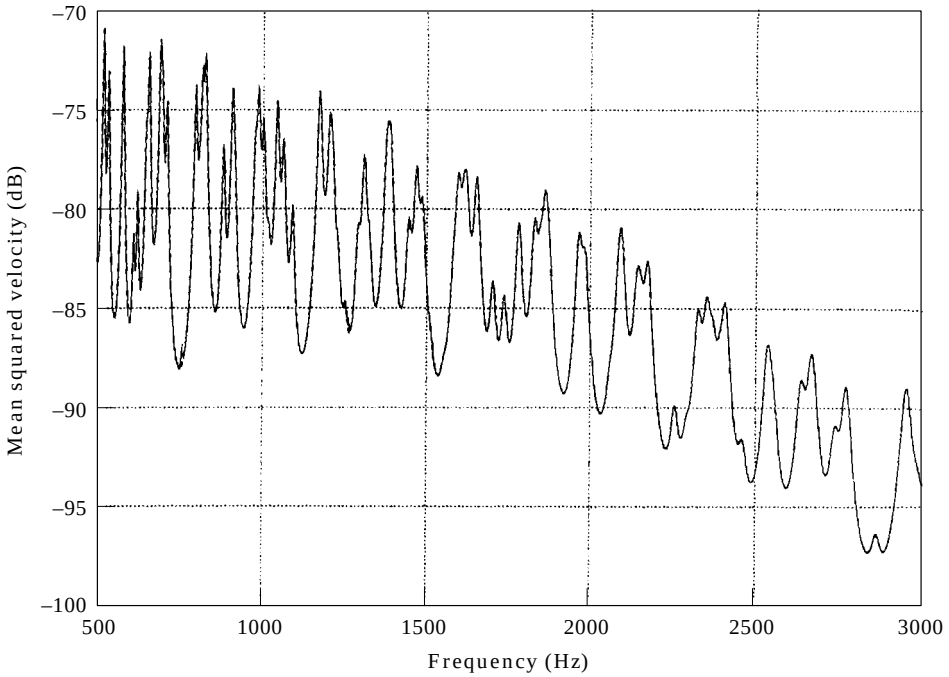

Figure 10. Comparison of the mean square velocity of the radiating, air loaded steel plate obtained by the proposed filter bank method (——) and by a direct method (——).

computed according to Appendix B. Therefore, the global solution obtained results from a smooth transition between the solutions computed for two successive subdomains.

To have a similar approximation with the direct frequency computation, one approach is to use a linearization of the system properties. Since the radiation effect is modelled as an impedance matrix whose coefficients result from Rayleigh integrals [12], such a mathematical study would be complicated. Another approach is to assume constant properties on different frequency bandwidths. Due to the linearization of the method presented, this latter approach requires very narrow bandwidths to have a similar solution quality, i.e., to avoid discontinuities. Thus, it is equivalent to a step by step frequency computation. However, computing the radiation coefficients at every frequency requires a large CPU time. The resolution presented computes these coefficients at the central frequencies only. Consequently, the method proposed is about 40 times faster in terms of CPU time than the direct method.

The number m_F of sampling values depending on frequency subdomains is given in Table 3. Large values of m_F are obtained in lower frequency ranges, i.e., below the critical frequency. This confirms the importance of the progressive frequency subdivision as regards to numerical requirements.

9. CONCLUSION

Using a classical matrix approach (F.E.M., B.E.M., semi-analytical methods, . . .), the aim of this paper was to propose an efficient numerical vibroacoustic method to compute the displacement field of a structure submitted to harmonic forces in the medium frequency range. The prsent method has been developed in continuation of the work of Soize [5, 6]. The dynamic equation is transformed into a set of time domain differential equations of motion by dividing the whole frequency range of interest into several frequency subdomains. The method consists of analysing the force signal to get its contribution on each frequency subdomain and then, to reconstruct the complete investigated displacement field from the different time domain solutions. The development was carried out within the framework of non-uniform modulated filter banks.

Because vibroacoustic indicators are evaluated in the frequency domain, low-pass analysis and synthesis filters have been designed to ensure a whole frequency decomposition and reconstruction. A prototype causal filter with compact time support (equation (19)) is proposed to define the analysis filter bank. The condition of frequency reconstruction (equation (10)) provides the synthesis filter bank. Using the presented analysis filters, no criterion is needed for the beginning of time domain integration. Furthermore, sampling values are computed at positive times only. To stop the time domain integration, a test on the first derivative of a cumulated dissipated power quantity (equation (23)) is proposed since signal energies are bounded. Consequently, the numerical computation of the time domain integration needs two numerical parameters, i.e., the time increment and an error value to stop the integration. These two parameters influence the quality of the signal response in relation to the numerical scheme used to solve the time domain equations.

Note that the time domain integration in the low frequency ranges needs too many CPU resources but, at these frequencies, modal or direct methods give excellent results. Therefore, greater benefits will be obtained if the presented computation method is applied to higher frequencies. This paper avoided the discussion of an appropriate description of the structure for the medium frequency range. On the one hand, the limitation of the method is related to the variational approach used to obtain the initial matrices. For instance, the mesh size of a finite element model as to be sufficiently small to accurately

capture the vibroacoustic displacement field. On the other hand, if one wants to consider the uncertainities of the dynamical behaviour of the structure, probability aspects could be introduced in the method.

It is emphasized here that the presented method deals with frequency dependent matrices. Therefore, the division of the complete frequency domain should be adapted to the fluctuations of the system properties. Furthermore, the efficiency of the presented method also depends on that division of the whole frequency domain into several subdomains. It has been found that progressively increasing frequency bandwidths gives better numerical performance. Hence, a non-uniform filter bank as shown in Figure 7 is proposed. Validations show that the method presented is very accurate.

Finally, two remarks are given about the signal processing aspects of the method. First, the progressive time-frequency mesh can be connected to a wavelet approach [13]. Second, the chosen framework of modulated filter banks allowed a complete time analysis to be given and therefore a time reconstruction could be investigated. These two points are appropriate for studying the dynamical behaviour of structures for the medium frequency range and call for further developments.

ACKNOWLEDGMENTS

The authors would like to thank Olivier Beslin for his helpful advices; André Côté and Patrice Masson for their good knowledge of the English language.

REFERENCES

1. P. Ladevèze 1996 *Comptes Rendus de l'Académie des Sciences* **322**, 849–856. A new computational approach for structure vibrations in the medium frequency range.
2. H. S. Kim, H. J. Kang and J. S. Kim 1994 *Journal of Sound and Vibration* **174**, 493–504. A vibration analysis of plates at high frequencies by the power flow method.
3. A. Carcaterra and A. Sestieri 1995 *Journal of Sound and Vibration* **188**, 269–282. Energy density equations and power flow in structures.
4. R. H. Lyon and R. G. DeJong 1995 *Statistical Energy Analysis*. London: Butterworth-Heinemann.
5. C. Soize 1982 *La recherche aérospatiale* **5**, 353–376. Vibrations linéaires moyennes fréquences des structures élastiques anisotropes.
6. C. Soize 1993 *Journal of the Acoustical Society of America* **94**, 849–865. A model and numerical method in the medium frequency range for vibroacoustic predictions using the theory of structural fuzzy.
7. N. Atalla and R. J. Bernhard 1994 *Applied Acoustics* **43**, 271–294. Review of numerical solutions for low-frequency structural-acoustic problems.
8. M. A. Bernier, N. Atalla 1997 *submitted to C.S.M.E*. Investigation of a dual time-frequency algorithms to solve linear structural dynamics systems.
9. P. P. Vaidyanathan 1990 *Proceedings of the IEEE Signal Processing*, **78**. Multirate digital filters, filter banks, polyphase networks, and applications: a tutorial.
10. K. Nayebi, T. P. Barnwell and M. J. T. Smith 1993 *IEEE Transactions on Signal Processing* **41**, 1114–1127. Nonuniform filter banks: a reconstruction and design theory.
11. S. Wada 1995 *IEEE Transactions on Circuits and Systems–II. Analog and Digital Signal Processing* **42**, 115–121. Design of non-uniform division multirate FIR filter banks.
12. N. Atalla and J. Nicolas 1994 *Journal of the Acoustical Society of America*, **95**, 3369–3378. A new tool for predicting rapidly and rigorously the radiation efficiency of plate-like structures.
13. I. Daubechies 1992 *Ten Lectures on Wavelets*. Philadelphia: Society for Industrial and Applied Mathematics.

APPENDIX A: CONDITION FOR FREQUENCY RECONSTRUCTION

The numerical resolution of equation (5) gives a set of time samples $\underline{u}_n(kT_n)$ to describe the solution $\underline{u}_n(t)$. A sampled signal $\underline{u}_n^e(t)$ is used to define this solution such that

$$\underline{u}_n^e(t) = \sum_k \underline{u}_n(kT_n)\delta(t - kT_n).$$

Using Poisson's formula, the Fourier transform $\underline{\hat{u}}_n^e(f)$ of $\underline{u}_n^e(t)$ is

$$\underline{\hat{u}}_n^e(f) = \frac{1}{T_n}\sum_k \underline{\hat{u}}_n\left(f - \frac{k}{T_n}\right).$$

If $\underline{\hat{u}}_n(f)$ is a low-pass signal cutting off at $\Delta f_n/2$, one can conclude that

$$\underline{\hat{u}}_n^e(f) = \frac{1}{T_n}\underline{\hat{u}}_n(f) \quad \forall f \in \left[-\frac{\Delta f_n}{2}, \frac{\Delta f_n}{2}\right].$$

The Fourier transform $\underline{\hat{x}}_n(f)$ of the time excitation (equations (6)) is $\underline{\hat{x}}_n(f) = \underline{\hat{x}}(f + f_n)\hat{g}_n(f)$.

Under these conditions, the equation of motion (4) becomes

$$[\hat{Z}_n(f)]T_n\underline{\hat{u}}_n^e(f) = \hat{g}_n(f)\underline{\hat{x}}(f + f_n), \quad \forall f \in \left[-\frac{\Delta f_n}{2}, \frac{\Delta f_n}{2}\right]. \tag{27}$$

The task is now to build the complete resulting equation of motion by adding the N equations given by equation (27) over the whole frequency domain. Using the property $[\hat{Z}_n(f - f_n)] = [\hat{Z}(f, f_n)]$, each frequency equation (27) is translated from f_n to zero and multiplied by $h_n(f)$. Hence, the addition of the N subdomains gives the frequency equation of motion (9) with

$$\underline{\hat{x}}^r(f) = \underline{\hat{x}}(f)\sum_{n=1}^{N} \hat{g}_n(f - f_n)\hat{h}_n(f - f_n).$$

It follows that $\underline{\hat{x}}^r(f)$ is constructed from $\underline{\hat{x}}(f)$ by applying the condition given by equation (10).

APPENDIX B: FREQUENCY RECONSTRUCTED DISPLACEMENT FIELD

Conditions given by equations (16)–(18) being verified, the frequency reconstructed displacement field $\underline{\hat{u}}^r(f)$ (equation (8)) is given by

$$\underline{\hat{u}}^r(f) = \frac{\underline{\hat{u}}_n(f - f_n)}{\hat{g}_n(f - f_n)}, \quad \forall f \in \left[f_n, f_{n+1} - \frac{\Delta f_{n+1}}{2}\right];$$

$$\underline{\hat{u}}^r(f) = \frac{\underline{\hat{u}}_n(f - f_n)\hat{g}_n^*(f - f_n)}{|\hat{g}_n(f - f_n)|^2 + |\hat{g}_{n+1}(f - f_{n+1})|^2} + \frac{\underline{\hat{u}}_{n+1}(f - f_{n+1})\hat{g}_{n+1}^*(f - f_{n+1})}{|\hat{g}_n(f - f_n)|^2 + |\hat{g}_{n+1}(f - f_{n+1})|^2},$$

$$\forall f \in \left]f_{n+1} - \frac{\Delta f_{n+1}}{2}, f_n + \frac{\Delta f_n}{2}\right[;$$

$$\hat{\underline{u}}^r(f) = \frac{\hat{\underline{u}}_{n+1}(f - f_{n+1})}{\hat{g}_{n+1}(f - f_{n+1})}, \quad \forall f \in \left[f_n + \frac{\Delta f_n}{2}, f_{n+1} \right[.$$

For identical width ($\Delta f_n = \Delta f_{n+1} = \Delta f$), the displacement field solution is given by

$$\hat{\underline{u}}^r(f) = \tfrac{1}{2}[\hat{\underline{u}}_n(f - f_n)\hat{g}(f - f_n) + \hat{\underline{u}}_{n+1}(f - f_{n+1})\hat{g}(f - f_{n+1})], \quad \forall f \in [f_n, f_{n+1}].$$

The frequency solution $\hat{\underline{u}}_n(f)$ is computed by using sampling values such that

$$\hat{\underline{u}}_n(f) = \sum_k \underline{u}_n(kT_n) \exp[-j2\pi f k T_n].$$